Dynamical analysis of a spinning solar sail

ARTICLE *in* ADVANCES IN SPACE RESEARCH · DECEMBER 2011

Impact Factor: 1.36 · DOI: 10.1016/j.asr.2011.06.012

3 AUTHORS, INCLUDING:

S p Gong
Tsinghua University
75 PUBLICATIONS **201** CITATIONS
SEE PROFILE

Li Junfeng
Tsinghua University
124 PUBLICATIONS **612** CITATIONS
SEE PROFILE

Available online at www.sciencedirect.com
ScienceDirect
Advances in Space Research 48 (2011) 1797–1809
ADVANCES IN SPACE RESEARCH (a COSPAR publication)
www.elsevier.com/locate/asr

Dynamical analysis of a spinning solar sail

Shengping Gong [a,*], Junfeng Li [a], Kaijian Zhu [b]

[a] School of Aerospace, Tsinghua University, Beijing 100084, China
[b] State Key Lab of Astronautical Dynamics, Xi'an Satellite Control Center, Xi'an 710043, China

Available online 26 June 2011

Abstract

This paper discusses the orbit and attitude dynamics of a solar sail, and gives the sufficient conditions of a stable orbit and attitude coupled system. The stability of the coupled system is determined by the orbit stability and attitude stability. Based on the sufficient conditions, a spin-stabilized solar sail of cone configuration is proposed to evolve in the heliocentric displaced orbit. For this kind of configuration, the attitude is always stable by spinning itself. The orbit stability depends on the orbit parameters of the heliocentric displaced orbit, the ratio of the orbit radius to displaced distance and orbit angular velocity. If the center of mass and center of pressure overlap, it can be proved that the coupled system is stable when the orbit parameters are chosen in the stable region. When the center of mass and center of pressure offset exists, the stability of the coupled system can not be judged. A numerical example is given and the result shows that both the orbit and attitude are stable for the case.

Keywords: Solar sail; Dynamics; Spinning

1. Introduction

Recently, attentions have been focused on solar sail missions, such as the new artificial Lagrange point created by solar sail to be used for NOAA/NASA/DOD to provide early warning of solar plasma storms, before they reach Earth (West, 1996; Prado et al., 1996). Sailcraft usually have a very large and complex structure, and conventional thrusters and reaction wheels are usually impractical or inefficient for the sailcraft control. Therefore, passive control is a good option; thus this paper investigates the passive stability of a sailcraft on a displaced solar orbit with the orbit and attitude considered simultaneously. Most literature deals with the orbit and attitude of the solar sails separately. The attitude is usually investigated solely, and the orbit control is investigated with the assumption that the attitude can be adjusted freely to control the orbit. However, the controlled attitude may lag behind the required attitude, and that may make the orbit unstable. In addition, the deviation from the reference orbit will influence the attitude. Therefore, the orbital dynamics and attitude dynamics should be coupled to analyze the orbit stability. A cone solar sail is proposed to evolve in a displaced solar orbit in this paper. Displaced solar orbits have been investigated for several years. Forward considered a displaced solar sail north or south of the geostationary ring (Forward, 1981). McInnes has done much work on the issue, in which large families of displaced orbits were investigated by considering the dynamics of a solar sail in a rotating frame (McInnes and Simmons, 1992). The dynamics, stability and control of different families of displaced orbits were investigated in detail (McInnes, 2002, 1998; McInnes and Macpherson, 1991; McInnes, 1999; McInnes and Simmons, 1992). Molostov investigated the displaced orbits when the solar sail with absorption is taken into account (Molostov and Shvartsburg, 1992a,b). Attitude dynamics is another very important issue for solar sails. Attitude stabilization of a space vehicle by solar radiation pressure was first proposed by Sohn (1959). Since

* Corresponding author.
E-mail addresses: gongsp@tsinghua.edu.cn, gsp04@mails.tsinghua.edu.cn (S. Gong), lijunf@tsinghua.edu.cn (J. Li), zhukj06@mails.tsinghua.edu.cn (K. Zhu).

0273-1177/$36.00 © 2011 COSPAR. Published by Elsevier Ltd. All rights reserved.
doi:10.1016/j.asr.2011.06.012

then, many researchers have investigated attitude stabilization of a satellite using solar radiation pressure. In fact, such a solar-pressure attitude control concept has been successfully implemented on a certain type of geostationary satellites as well as several interplanetary spacecraft (Acord and Nicklas, 1964). However, attitude control of a sailcraft is different from the solar-pressure attitude control for ordinary spacecraft. Recently, several attitude control strategies for solar sails have been proposed. The attitude dynamics and control of solar sails using a gimbaled control boom were investigated by Benjamin (2001). The gimbaled control boom and sail control vanes were discussed in detail (Bong, 2004), and multiple simulations were given for various sail missions. In Bong (2004), the control system uses two ballast masses running along the mast for pitch/yaw control and roll stabilizer bars at the mast tips for quadrant tilt control. The second strategy employed a micro-pulsed plasma thruster mounted at the mast tips for attitude control. Passive control of an interplanetary spacecraft was discussed in Acord and Nicklas (1964) and passive control of the solar sail on the displaced solar orbit was investigated in McInnes (1998). The results show that the solar displaced orbits are stable if the sail pitch angle is fixed with respect to the rotating frame.

Firstly, the criterion of judging the stability of attitude and orbit dynamics of a general solar sail is discussed. Then, we propose a solar sail of a cone shape. The attitude of the sail can be spin-stabilized while the stability of the orbit depends on the orbit parameters, where stable region in the parameter space is given. The center of mass of the sail and center of pressure of the sail is denoted as cm and cp, respectively. If no cm/cp offset exists, the attitude and orbit coupled system is stable according to the criterion. If cm/cp offset exists, analytical method can not handle the stability analysis and two numerical simulations are used to check the stability of the coupled system. The nomenclatures used in this paper are given in Table 1.

Table 1
Nomenclatures.

$\boldsymbol{r}$	Position vector of the sail with respect to the Sun
$\dot{\boldsymbol{r}}$	Velocity vector of the sail with respect to the Sun
$\boldsymbol{\chi}$	Euler angles used to describe the attitude of the sail with respect to a reference frame
$\boldsymbol{\Omega}$	Angular velocity of a general sail
$\boldsymbol{\omega}$	Angular velocity of a spinning sail
Γ	Function used to describe the orbit dynamics of the solar sail
$\boldsymbol{\Delta}$	Function used to describe the attitude dynamics of the sail
Π	Function used to describe the kinematics
$\mathbf{B}_i\ (i = 1, \ldots, 9)$	A 3×3 matrix
$\lambda_i (i = 1, \ldots, 12)$	Eigenvalue of coefficient matrix of linearized coupled dynamic equation
λ_a	Eigenvalue of coefficient matrix of linearized attitude dynamic equation
λ_o	Eigenvalue of coefficient matrix of linearized orbit dynamic equation
$\mathbf{E}$	Identity matrix
ρ	Radius of the heliocentric displaced solar orbit
ϑ	Polar angle of the sail
z	Displaced height of the heliocentric displaced solar orbit
$\boldsymbol{a}_s$	Solar radiation pressure acceleration
$\boldsymbol{n}_s$	Unit vector of the sunlight direction
$\boldsymbol{n}_i$	Unit vector of the normal of an infinitesimal fan
γ	Angle between the sunlight direction and Z axis at the position of the sail
β	Lightness number of the solar sail
AU	A astronomical unit
P_0	Solar radiation pressure at the distance of one astronomical unit from the Sun
$\boldsymbol{r}_{\mathrm{pm}}$	A vector of pressure center relative to mass center
$\boldsymbol{M}_s$	Solar radiation pressure torques (SRPT) exerted on the solar sail
$\boldsymbol{F}_s$	Solar radiation pressure Forces (SRPF) exerted on the solar sail
l	Slant height of the cone sail
ε	Half vertex angle of the cone
m	Mass of the solar sail
ξ	Angle between a generatrix and X axis
μ	Gravitational constant of the Sun
σ	Mass-to-area ratio of the sail
φ, θ, ψ	Three Euler angles from the orbital frame to the body frame
ω_{s}	Spin angular velocity of the sail
ω_{E}	Angular velocity of the earth around the sun
ω_0	Reference angular velocity of the displaced solar orbit
$\mathbf{I}$	Inertia matrix of the sail
$\eta_{\mathrm{i}}\ (i = 1, \ldots, 3)$	The component of the cm/cp offset in the body-fixed frame
Superscript b	Projection of a vector in the body-fixed frame
Superscript o	Projection of a vector in the orbital frame
Subscript 0	Value for the variable in the equilibrium position
Subscripts ρ, ϑ, z	A component of the vector in the corresponding direction
Prefix δ	Variation with respect to a variable
Prefix d	Differential with respect to a variable

2. Orbit and attitude dynamics of a general sail

Here the stability of an equilibrium point using the attitude and orbit coupled dynamic system is discussed. Euler angles are used to describe the attitude of the solar sail. No singular problem appears since the stability analysis assumes a small variation of the attitude. The orbit dynamical equation is written as:

$$\ddot{\boldsymbol{r}} = \boldsymbol{\Gamma}(\boldsymbol{r}, \boldsymbol{\chi}, \dot{\boldsymbol{r}}, \boldsymbol{\Omega}). \tag{1}$$

If a cp/cm offset exists for the solar sail, there will be a SRPT (solar radiation pressure torque) that depends on the sail attitude. In this case, attitude dynamics can be written as:

$$\dot{\boldsymbol{\Omega}} = \boldsymbol{\Delta}(\boldsymbol{r}, \boldsymbol{\chi}, \boldsymbol{\Omega}). \tag{2}$$

The corresponding kinematic equation is given by

$$\dot{\boldsymbol{\chi}} = \boldsymbol{\Pi}(\boldsymbol{\chi}, \boldsymbol{\Omega}), \tag{3}$$

where $\boldsymbol{\Pi}$ depends on the rotation sequences from the orbit reference frame to the body fixed reference frame.

Assume that position equilibrium point $\boldsymbol{r}_0$, and attitude equilibrium point $\boldsymbol{\chi}_0$ exist for the dynamics equations. It means that $\boldsymbol{r}_0$ and $\boldsymbol{\chi}_0$ satisfy the following equations:

$$\begin{cases} \boldsymbol{\Gamma}(\boldsymbol{r}_0, \boldsymbol{\chi}_0, 0, \boldsymbol{\Omega}_0) = 0, \\ \boldsymbol{\Pi}(\boldsymbol{\chi}_0, \boldsymbol{\Omega}_0) = 0, \\ \boldsymbol{\Delta}(\boldsymbol{r}_0, \boldsymbol{\chi}_0, \boldsymbol{\Omega}_0) = 0, \end{cases} \tag{4}$$

Eq. (4) gives the force balance and torque balance conditions. The linear stability of the coupled equilibrium point is investigated here. This is achieved in the usual manner by linearizing the equations of motion about the nominal solution to obtain a variational equation. The stability of the orbit and attitude coupled system may then be determined by examining the eigenvalues of characteristic equation. The nonlinear equation of motion will be linearized by perturbing the sail from its nominal orbit and nominal attitude. It should be noted that only a linear analysis is performed, which in the present case provides necessary conditions for stability and sufficient conditions for instability:

$$\begin{cases} \delta\ddot{\boldsymbol{r}} = \frac{\partial \boldsymbol{\Gamma}}{\partial \boldsymbol{r}}\Big|_{\substack{r=r_0 \\ \chi=\chi_0}} \delta\boldsymbol{r} + \frac{\partial \boldsymbol{\Gamma}}{\partial \boldsymbol{\chi}}\Big|_{\substack{r=r_0 \\ \chi=\chi_0}} \delta\boldsymbol{\chi} + \frac{\partial \boldsymbol{\Gamma}}{\partial \dot{\boldsymbol{r}}}\Big|_{\substack{r=r_0 \\ \chi=\chi_0}} \delta\dot{\boldsymbol{r}} + \frac{\partial \boldsymbol{\Gamma}}{\partial \boldsymbol{\Omega}}\Big|_{\substack{r=r_0 \\ \chi=\chi_0}} \delta\boldsymbol{\omega} = \mathbf{B}_1\delta\boldsymbol{r} + \mathbf{B}_2\delta\boldsymbol{\chi} + \mathbf{B}_3\delta\dot{\boldsymbol{r}} + \mathbf{B}_4\delta\boldsymbol{\Omega}, \\ \delta\dot{\boldsymbol{\chi}} = \frac{\partial \boldsymbol{\Pi}}{\partial \boldsymbol{\chi}}\Big|_{\substack{r=r_0 \\ \chi=\chi_0}} \delta\boldsymbol{\chi} + \frac{\partial \boldsymbol{\Pi}}{\partial \boldsymbol{\Omega}}\Big|_{\substack{r=r_0 \\ \chi=\chi_0}} \delta\omega = \mathbf{B}_5\delta\boldsymbol{\chi} + \mathbf{B}_6\delta\boldsymbol{\Omega}, \\ \delta\dot{\boldsymbol{\Omega}} = \frac{\partial \Delta}{\partial \boldsymbol{r}}\Big|_{\substack{r=r_0 \\ \chi=\chi_0 \\ \Omega=\Omega_0}} \delta\boldsymbol{r} + \frac{\partial \Delta}{\partial \boldsymbol{\chi}}\Big|_{\substack{r=r_0 \\ \chi=\chi_0 \\ \Omega=\Omega_0}} \delta\boldsymbol{\chi} + \frac{\partial \Delta}{\partial \boldsymbol{\Omega}}\Big|_{\substack{r=r_0 \\ \chi=\chi_0 \\ \Omega=\Omega_0}} \delta\boldsymbol{\Omega} = \mathbf{B}_7\delta\boldsymbol{r} + \mathbf{B}_8\delta\boldsymbol{\chi} + \mathbf{B}_9\delta\boldsymbol{\Omega}, \end{cases} \tag{5}$$

where $\mathbf{B}_i$ $(i = 1, 2, \ldots, 9)$ is 3×3 matrices. Let $\boldsymbol{S} = [\,\delta\boldsymbol{r} \quad \delta\dot{\boldsymbol{r}} \quad \delta\boldsymbol{\chi} \quad \delta\boldsymbol{\Omega}\,]^T$, the variational equation can be written as:

$$\dot{\boldsymbol{S}} = \begin{bmatrix} 0 & \mathbf{E} & 0 & 0 \\ \mathbf{B}_1 & \mathbf{B}_2 & \mathbf{B}_3 & \mathbf{B}_4 \\ 0 & 0 & \mathbf{B}_5 & \mathbf{B}_6 \\ \mathbf{B}_7 & 0 & \mathbf{B}_8 & \mathbf{B}_9 \end{bmatrix} \quad S = \mathbf{H}S. \tag{6}$$

Let λ_i $(i = 1, \ldots, 12)$ be the eigenvalues of matrix $\mathbf{H}$. Define a characteristic parameter as:

$$\Xi = \max_{i=1\ldots12} Re(\lambda_i). \tag{7}$$

The following conclusions can be drawn based on the Lyapunov theory: the coupled equilibrium point is asymptotically stable when $\Xi < 0$; the equilibrium point is stable when $\Xi = 0$; the equilibrium point is unstable when $\Xi > 0$.

Therefore, a sufficient condition that guarantees the stability of the coupled equilibrium point can be given by

$$\begin{cases} \boldsymbol{\Pi}(\boldsymbol{\chi}_0, \boldsymbol{\Omega}_0) = 0, \\ \boldsymbol{\Delta}(\boldsymbol{r}_0, \boldsymbol{\chi}_0, \boldsymbol{\Omega}_0) = 0, \\ \boldsymbol{\Gamma}(\boldsymbol{r}_0, \boldsymbol{\chi}_0, \dot{\boldsymbol{\Omega}}_0) = 0, \\ \Xi \leqslant 0. \end{cases} \tag{8}$$

Usually, the orbit of a regular spacecraft does not influence its attitude. Here, the solar sail orbit influences the attitude through the SRPT, which depends on the sail attitude and the distance from the Sun. For the discussion of equilibrium stability, the SRPT variation caused by the distance variation is very small compared with the variation caused by body rotation. Firstly, we assume that the attitude of the sail is independent of the orbit and only the orbit depends on the attitude. In this case, the stability of the attitude equilibrium point can be checked without consideration of the orbit. Euler angles and angular velocity perturbations are introduced to obtain the variational equation. The stability is determined by the eigenvalues of coefficient matrix of the linearized equation:

$$\left|\lambda_a\mathbf{E} - \begin{bmatrix} \mathbf{B}_5 & \mathbf{B}_6 \\ \mathbf{B}_8 & \mathbf{B}_9 \end{bmatrix}\right| = k_a \prod_{i=1}^{6} \left(\lambda_a - \lambda_a^i\right). \tag{9}$$

The orbit stability can be checked assuming that the attitude is in equilibrium, namely $\boldsymbol{\chi} = \boldsymbol{\chi}_0$. The equation of motion is linearized by introducing a perturbation, $\boldsymbol{r} = \boldsymbol{r}_0 + \delta\boldsymbol{r}$. Similarly, the stability is determined by the eigenvalues of the coefficient matrix that is given by

$$\left|\lambda_o\mathbf{E} - \begin{bmatrix} 0 & \mathbf{E} \\ \mathbf{B}_1 & \mathbf{B}_3 \end{bmatrix}\right| = k_o \prod_{i=1}^{6} \left(\lambda_o - \lambda_o^i\right). \tag{10}$$

For the orbit and attitude coupled dynamics, the variational equation is obtained by introducing the perturbations, $\boldsymbol{r} = \boldsymbol{r}_0 + \delta\boldsymbol{r}$ and $\boldsymbol{\chi} = \boldsymbol{\chi}_0 + \delta\boldsymbol{\chi}$. With the assumption that the attitude is independent of the orbit, the coefficient matrix of the linearized equation is obtained by taking $\mathbf{B}_7$ in $\mathbf{H}$ to be zero. Similarly, the stability of the coupled equilibrium point is obtained by checking the eigenvalues of the coefficient matrix, given by

$$\begin{aligned} |\lambda_c\mathbf{E} - \mathbf{H}| &= \left|\lambda_c\mathbf{E} - \begin{bmatrix} \mathbf{B}_5 & \mathbf{B}_6 \\ \mathbf{B}_8 & \mathbf{B}_9 \end{bmatrix}\right| \left|\lambda_c\mathbf{E} - \begin{bmatrix} 0 & \mathbf{E} \\ \mathbf{B}_1 & \mathbf{B}_3 \end{bmatrix}\right| \\ &= k_a k_o \prod_{i=1}^{6} \left(\lambda_c - \lambda_o^i\right)\left(\lambda_c - \lambda_a^i\right). \end{aligned} \tag{11}$$

The eigenvalues of $\mathbf{H}$ is composed of λ_a and λ_o. Therefore, the stability of the coupled equilibrium point

is determined by the stability of orbit equilibrium point and stability of the attitude equilibrium point, respectively. The coupled equilibrium point is asymptotically stable when both the orbit and attitude equilibrium points are asymptotically stable. The coupled equilibrium point is stable when both the orbit and attitude equilibrium points are stable or one is stable and the other is asymptotically stable. The coupled equilibrium point is unstable when either of the orbit or attitude equilibrium points is unstable. This criterion is used to judge the stability of the coupled system when the attitude is independent of the orbit.

3. Heliocentric displaced orbit

A two body model is used, where only the solar gravity and solar radiation pressure force exerted on the solar sail are taken into account. Two frames are defined to describe the orbit dynamics of the solar sail. The inertial frame $OXYZ$ is defined as: the origin is at the Sun; the X axis points to the J2000 Equinox; Z axis is perpendicular to the ecliptic plane, and Y axis forms a right triad with the X and Z axes. The orbital frame $Oxyz$ is defined as: the origin is also at the Sun; the x axis points to projection point of the solar sail in the ecliptic plane, the z axis is consistent with the Z axis, and y forms a right triad with the x and z axes. The dynamical equation of motion for the sail is given in the orbit frame. The cylindrical coordinates instead of Cartesian coordinates are used to describe the states of the sail, where ρ is the distance from the sail to the z axis, and ϑ is the angle between the x axis and X axis, z is the distance between the sail and the ecliptic plane. The transformation between the Cartesian coordinates and cylindrical coordinates is given by

$$\begin{cases} X = \rho\cos\vartheta, \\ Y = \rho\sin\vartheta, \\ Z = z. \end{cases} \tag{12}$$

The orbit dynamic equations in the orbital frame are written as (McInnes, 1997):

$$\begin{cases} \ddot{\rho} - \rho\dot{\vartheta}^2 = -\frac{\mu}{r^3}\rho + a^o_{s\rho}, \\ \ddot{\vartheta} + 2\frac{\dot{\rho}\dot{\vartheta}}{\rho} = a^o_{s\vartheta}, \\ \ddot{z} = -\frac{\mu}{r^3}z + a^o_{sz}. \end{cases} \tag{13}$$

The equilibrium point in the rotating frame $Oxyz$ is a heliocentric displaced solar orbit in the inertial frame. To keep the sail on the orbit, the sail must rotate once per orbit with respect to an inertial frame. The SRPF required for a displaced Sun-centered orbit of radius ρ_0, displacement z_0 and orbital angular velocity ω_0 are given by McInnes (1997)

$$\begin{cases} a^o_{s\rho} = (\tilde{\omega}^2 - \omega_0^2)\rho_0, \\ a^o_{s\vartheta} = 0, \\ a^o_{sz} = \tilde{\omega}^2 z_0, \end{cases} \tag{14}$$

where $\tilde{\omega} = \sqrt{\mu/(\rho_0^2 + z_0^2)^3}$.

4. Sail configuration design and dynamical equations

In this section we discuss the design method to choose the sail parameters that satisfy the force and torque balance. The sail parameters are completely determined by the displaced solar orbit. For a designed solar sail, the attitude dynamic and kinematic equations are given. These equations will be used for stability analysis in next section.

4.1. Sail configuration

A sail with a cone shape is chosen to discuss the attitude and orbit stability, as shown in Fig. 1. The advantage of this configuration is that the attitude can be spin-stabilized and provide a component for generating a displaced solar orbit around the sun. In addition, not only the attitude but the orbit is stabilized by spinning the sail configuration for some displaced solar orbits, which is the original idea of this paper. However, this configuration reduces the efficiency of the sail film. A much bigger sail is required to provide the same acceleration of a flat sail. Moreover, the difficulty of building and deploying this kind of shape is not clear. The half vertex angle and the slant height are two important parameters to be determined for this sail, where the half vertex angle determines the efficiency of the sail and the slant height determines the total area for a given half vertex angle. The effective area is equal to the base area as the sunlight is along the symmetry axis. The base area is $\pi l^2 \sin^2\varepsilon$ and the slanted area is $\pi l^2 \sin\varepsilon$. Therefore, the sail film surface efficiency utilization ratio is $\sin\varepsilon$. In this paper, the slant height and mass-to-area ratio are designed to satisfy the force balance conditions. The conditions determine the two parameters completely for a given displaced solar orbit. There are no free parameters to design for the stability conditions. Therefore, the coupled orbit and attitude dynamics of the designed sail are analyzed for different orbits.

A body fixed frame is defined to calculate the SRPF and SRPT exerted on the sail for a given attitude status. The

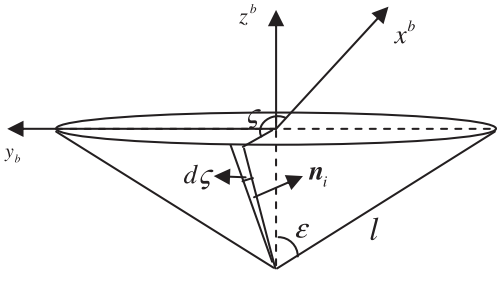

Fig. 1. Cone-shaped solar sail.

origin is at the center of mass of the sail, the z^b axis is along the symmetry axis of the cone, the x^b axis lies in the plane of x and z axes (along the x axis when the sail is in equilibrium), the y^b axis forms a right-handed triad with the x^b and z^b axes. Then, the relative orientation of the sailcraft, with respect to the orbital frame, is described by three Euler angles (ϕ, θ, ψ) of the rotational sequence of $R_3(\psi) \leftarrow R_1(\theta) \leftarrow R_2(\phi)$ from the orbital frame to the body-fixed frame. The transformation matrix can be given by

$$A_{213} = R_3(\psi)R_1(\theta)R_2(\phi). \tag{15}$$

The cone is symmetric with respect to the z^b axis. Seen from the orbit frame, the rotation along the symmetry axis does not change the SRPF exerted on the solar sail. A transformation matrix, used to calculate the SRPF in the orbit frame, is defined as:

$$A_{21} = R_1(\theta)R_2(\phi). \tag{16}$$

The sunlight vector is assumed to be along the Sun-sail direction and it can be expressed in the orbital frame as:

$$\boldsymbol{n}_s^o = [\cos\gamma \quad 0 \quad \sin\gamma]^T, \quad \tan\gamma = \frac{x}{z}. \tag{17}$$

A phase angle ζ between a generatrix of the cone and the x^b axis is used to determine the position of the generatrix. Then, the normal unit vector of the generatrix in the body fixed frame can be given by

$$\boldsymbol{n}_i^b = [-\cos\varepsilon\cos\varsigma \quad -\cos\varepsilon\sin\varsigma \quad \sin\varepsilon]^T. \tag{18}$$

Consider an infinitesimal fan facing the sunlight. We can calculate the corresponding infinitesimal SRPF as:

$$\begin{aligned} d\boldsymbol{F}_s^o &= P_0\frac{AU^2}{r^2}\left(\boldsymbol{n}_s^o\cdot\boldsymbol{n}_i^o\right)^2\boldsymbol{n}_i^o ds \\ &= P_0\frac{AU^2}{r^2}\frac{l^2}{2}\left(\boldsymbol{n}_s^o\cdot\boldsymbol{n}_i^o\right)^2\boldsymbol{n}_i^o d\varsigma. \end{aligned} \tag{19}$$

If the symmetry axis is along the Z axis and sail is in the ecliptic plane, there will be half of the surface immersed in the sunlight. For a displaced orbit of small displaced height, the immersed area is slightly different. This paper focuses on the displaced orbit of small displaced height. In addition, since the radial axis of orbit frame is defined by the Sun-sail axis, the surface immersed in the sunlight can be determined by the phase angle range $\varsigma \in (\pi/2 \quad 3\pi/2)$. Integration of Eq. (19) along the surface in the sunlight yields:

$$\begin{aligned} \boldsymbol{F}_s^o &= P_0\frac{AU^2}{r^2}\int_{\pi/2}^{3\pi/2}\frac{l^2}{2}\left(\boldsymbol{n}_s^o\cdot\boldsymbol{n}_i^o\right)^2\boldsymbol{n}_i^o d\varsigma \\ &= P_0\frac{AU^2}{r^2}\frac{l^2}{2}\int_{\pi/2}^{3\pi/2}\left(\boldsymbol{n}_s^o\cdot A_{21}^T\boldsymbol{n}_i^b\right)^2 A_{21}^T\boldsymbol{n}_i^b d\varsigma. \end{aligned} \tag{20}$$

The SRPT can be given in the body-fixed frame as:

$$\boldsymbol{M}_s^b = \boldsymbol{r}_{pm}^b \times A_{213}\boldsymbol{F}_s^o. \tag{21}$$

Eqs. (20) and (21) can be integrated analytically. The expressions are complex, and they are not given here. If the orbit frame and body-fixed frame coincide, the expressions are simplified greatly:

$$\boldsymbol{F}_s^o = P_0\frac{AU^2}{r^2}\frac{l^2}{2}\begin{bmatrix} 2\cos^2\gamma\sin^2\varepsilon\cos\varepsilon + \frac{4}{3}\sin^2\gamma\cos^3\varepsilon + \pi\sin\gamma\cos\gamma\sin\varepsilon\cos^2\varepsilon \\ 0 \\ \pi\cos^2\gamma\sin^3\varepsilon + 4\sin\gamma\cos\gamma\sin^2\varepsilon\cos\varepsilon + \frac{\pi}{2}\sin^2\gamma\sin\varepsilon\cos^2\varepsilon \end{bmatrix} = \begin{bmatrix} \frac{Q_\rho}{r^2} \\ 0 \\ \frac{Q_z}{r^2} \end{bmatrix}, \tag{22}$$

$$\boldsymbol{M}_s^b = P_0\frac{AU^2}{r^2}\frac{l^2}{2}\begin{bmatrix} -2\eta_3\cos^2\gamma\sin^2\varepsilon\cos\varepsilon\cos\varsigma_0 - 4\eta_2\sin\gamma\cos\gamma\sin^2\varepsilon\cos\varepsilon\sin\varsigma_0 \\ -\frac{2}{3}\eta_3\sin^2\gamma\cos^3\varepsilon\cos^3\varsigma_0 + \frac{\pi}{2}\eta_2\sin^2\gamma\sin\varepsilon\cos^2\varepsilon + \pi\eta_2\cos^2\gamma\sin^3\varepsilon \\ 4\eta_1\sin\gamma\cos\gamma\sin^2\varepsilon\cos\varepsilon\sin\varsigma_0 - 2\eta_3\cos^2\gamma\sin^2\varepsilon\cos\varepsilon\sin\varsigma_0 - \frac{2}{3}\eta_3\sin^2\gamma\cos^3\varepsilon\sin\varsigma_0\cos^2\varsigma_0 \\ -\pi\eta_1\cos^2\gamma\sin^3\varepsilon - \frac{\pi\eta_1}{2}\sin^2\gamma\sin\varepsilon\cos^2\varepsilon + \pi\eta_3\sin\gamma\cos\gamma\sin\varepsilon\cos^2\varepsilon - \frac{4\eta_3}{3}\sin^2\gamma\cos^3\varepsilon\sin\varsigma_0 \\ -\pi\eta_2\sin\gamma\cos\gamma\sin\varepsilon\cos^2\varepsilon + 2\eta_1\cos^2\gamma\sin^2\varepsilon\cos\varepsilon\cos\varsigma_0 + 2\eta_2\cos^2\gamma\sin^2\varepsilon\cos\varepsilon\sin\varsigma_0 \\ +\frac{2\eta_1}{3}\sin^2\gamma\cos^3\varepsilon\cos^3\varsigma_0 + \frac{2\eta_2}{3}\sin^2\gamma\cos^3\varepsilon\sin\varsigma_0\cos^2\varsigma_0 + \frac{4\eta_2}{3}\sin^2\gamma\cos^3\varepsilon\sin\varsigma_0 \end{bmatrix}. \tag{23}$$

There are two design parameters, l and ε, that can be used to satisfy the force balance of solar sail in the displaced solar orbit. The design process is given in the next subsection.

4.2. Solar sail in displaced solar orbit

The SRPF generated by the solar sail can be used to displace the solar sail above the ecliptic plane. To levitate a displaced orbit with a radius of ρ_0, height z_0, and orbital angular velocity ω_0, the SRPF should satisfy the force conditions, given by Eq. (14). Consideration on the direction of the SRPF and required force yields:

$$\boldsymbol{F}_s^o = \begin{bmatrix} ma_{s\rho}^o & 0 & ma_{sz}^o \end{bmatrix}^T. \tag{24}$$

If the sail is in the displaced orbit, the sunlight direction can be described by the orbit radius and displaced distance:

$$\tan\gamma_0 = \frac{\rho_0}{z_0}. \tag{25}$$

The half vertex cone angle is chosen to satisfy the direction condition. Combination of Eqs. (14), (24), and (25) yields:

$$C_0\tan^3\varepsilon + C_1\tan^2\varepsilon + C_2\tan\varepsilon + C_3 = 0, \tag{26}$$

where

$$\begin{aligned} C_0 &= \pi\tan\gamma_0\left[1-\left(\frac{\omega_0}{\tilde{\omega}}\right)^2\right],\\ C_1 &= 4\tan^2\gamma_0\left[1-\left(\frac{\omega_0}{\tilde{\omega}}\right)^2\right]-2,\\ C_2 &= \frac{\pi}{2}\tan^3\gamma_0\left[1-\left(\frac{\omega_0}{\tilde{\omega}}\right)^2\right]-\pi\tan\gamma_0,\\ C_3 &= -\frac{4}{3}\tan^2\gamma_0. \end{aligned} \tag{27}$$

The root is only meaningful for the cases of $\tan\varepsilon > 0$. Therefore, the necessary and sufficient condition of existence of the physical design is that one positive root exists for the cubic equation at least. No design solution exists if no positive root exists. The roots are determined by two parameters, $\omega_0/\tilde{\omega}$ and γ_0. Fig. 2 gives the boundary of existing positive roots in $\omega_0/\tilde{\omega} - \gamma_0$ space and the boundary is a line given by $\omega_0/\tilde{\omega} = 1$. If $\omega_0/\tilde{\omega} > 1$, no positive root exists. When positive roots exist, the roots illustrate the shape of the cone, where $\varepsilon = 90°$ means that the cone degrade to a circle and $\varepsilon = 0$ degrades to a spacecraft with no SRPF. For a given ratio of the orbit radius to displaced height, the half vertex angle increases as the ratio of ω_0 to $\tilde{\omega}$ approaches one. For a given ratio of ω_0 to $\tilde{\omega}$, the half vertex angle decreases with ratio of orbit radius to displaced height. The results are reasonable from the point of view of qualitative analysis. The extreme case of $\gamma_0 = 90°$ corresponds to a keplerian circular orbit in ecliptic plane, and no out-of-plane force is required which corresponds to the design of $\varepsilon = 0$. The extreme case of $\gamma_0 = 0$ corresponds to an equilibrium point above north pole of the Sun, and only out-of-plane force is required, which can be realized by designing the area-to-mass ratio for a given ε as long as the symmetry axis of the cone is along z-axis. But the solution can not be obtained from Eq. (26) since all coefficients are zero. The variation of γ_0 from 90° to 0 leads to the change of ε from 0 to 90°. For a given orbit size, increment of orbit angular velocity leads to the decrement of the required force in the ecliptic plane, which is equivalent to the decrement of γ_0.

Besides the direction of the SRPF, the magnitude of the SRPF should match the requirement. According to Eqs. (14), (24), and (22), the condition of magnitude requirement can be expressed as:

$$ma_{s\rho}^o = \frac{P_0AU^2l^2}{2r^2}\left(2\cos^2\gamma\sin^2\varepsilon\cos\varepsilon + \frac{4}{3}\sin^2\gamma\cos^3\varepsilon + \pi\sin\gamma\cos\gamma\sin\varepsilon\cos^2\varepsilon\right). \tag{28}$$

The area of the cone is $\pi l^2\sin\varepsilon$. The mass-to-area ratio of the sail is obtained as:

$$\sigma = \frac{m}{\pi l^2\sin\varepsilon} = \frac{P_0AU^2}{2\pi a_{s\rho}^o r^2}\left(2\cos^2\gamma\sin\varepsilon\cos\varepsilon + \frac{4}{3}\sin^2\gamma\cos^3\varepsilon/\sin\varepsilon + \pi\sin\gamma\cos\gamma\cos^2\varepsilon\right). \tag{29}$$

For a pair of $\omega_0/\tilde{\omega}$ and γ_0, the half vertex angle is determined from Eq. (26). Therefore, the mass-to-area ratio depends on $\omega_0/\tilde{\omega}$, γ_0 and r. For a given displaced orbit, the lightness number β of a solar sail can be calculated (McInnes, 1998). Fig. 3 gives the ratio and the corresponding lightness number for different $\omega_0/\tilde{\omega}$ and γ_0 when

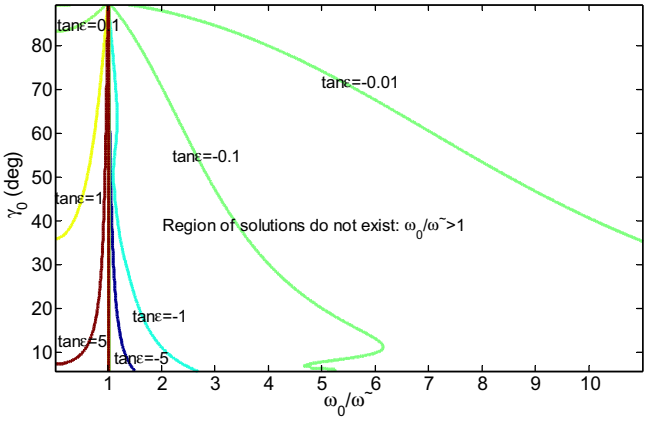

Fig. 2. The contour of half vertex angle of the cone.

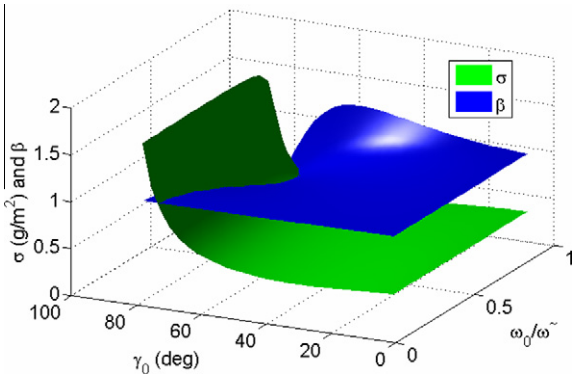

Fig. 3. The mass-to-area for different orbit.

$r = 0.98$ AU. The ratio almost keeps constant as $\omega_0/\tilde{\omega}$ varies and increases shapely as γ_0 increases. It seems that a large half vertex angle leads to high efficient utilization of the sail material and leads to a large mass-to-area ratio. However, a large half vertex angle corresponds to a small mass-to-area ratio here. This is because the sail lightness number required decreases greatly as γ_0 increases, as show in Fig. 3.

4.3. Attitude dynamics of the solar sail

According to the definition of orbital frame and body-fixed frame and the rotation sequences from the orbital frame to body fixed frame, $R_3(\psi) \leftarrow R_1(\theta) \leftarrow R_2(\varphi)$, the angular velocity of the sail can be written as the summation of the orbital angular velocity and solar sail angular velocity relative to the orbital frame. Therefore, the angular velocity components of the sailcraft in body-fixed frame can be given by

$$\boldsymbol{\omega}^b = \begin{bmatrix} \omega_x^b \\ \omega_y^b \\ \omega_z^b \end{bmatrix} = \begin{bmatrix} \dot{\phi}\sin\phi\cos\theta + \dot{\theta}\cos\psi \\ \dot{\phi}\cos\phi\cos\theta - \dot{\theta}\sin\psi \\ \dot{\psi} - \sin\theta\dot{\phi} \end{bmatrix} + A_{213}\begin{bmatrix} 0 \\ 0 \\ \dot{\vartheta} \end{bmatrix}. \tag{30}$$

Let $\boldsymbol{\chi} = [\,\phi \quad \theta \quad \psi\,]^T$, and denote $\sin\theta$ and $\cos\theta$ by s_θ and c_θ, respectively. Then, the kinematical differential equation can be derived from Eq. (30) as:

$$\dot{\boldsymbol{\chi}} = \begin{bmatrix} \dot{\phi} \\ \dot{\theta} \\ \dot{\psi} \end{bmatrix} = \frac{1}{c_\theta}\begin{bmatrix} \left(\omega_x^b + \dot{\vartheta}s_\phi c_\psi - \dot{\vartheta}\mathrm{s}_\psi \mathrm{s}_\theta c_\phi\right)\mathrm{s}_\psi + \left(\omega_y^b - \dot{\vartheta}s_\psi s_\phi - \dot{\vartheta}c_\psi c_\phi \mathrm{s}_\theta\right)\mathrm{c}_\psi \\ \left(\omega_x^b + \dot{\vartheta}s_\phi c_\psi - \dot{\vartheta}\mathrm{s}_\psi \mathrm{s}_\theta c_\phi\right)\mathrm{c}_\psi c_\theta - \left(\omega_y^b - \dot{\vartheta}s_\psi s_\phi - \dot{\vartheta}c_\psi c_\phi \mathrm{s}_\theta\right)s_\psi c_\theta \\ \left(\omega_x^b + \dot{\vartheta}s_\phi c_\psi - \dot{\vartheta}\mathrm{s}_\psi \mathrm{s}_\theta c_\phi\right)s_\theta s_\psi + \left(\omega_y^b - \dot{\vartheta}s_\psi s_\phi - \dot{\vartheta}c_\psi c_\phi \mathrm{s}_\theta\right)c_\psi s_\theta + \left(\omega_z^b - \dot{\vartheta}\mathrm{c}_\theta c_\phi\right)c_\theta \end{bmatrix}. \tag{31}$$

In the body-fixed frame, the attitude equation of motion can be given as:

$$\boldsymbol{I}\dot{\boldsymbol{\omega}}^b + \boldsymbol{\omega}^b \times (\boldsymbol{I}\cdot\boldsymbol{\omega}^b) = \boldsymbol{M}_s^b. \tag{32}$$

Eqs. (31) and (32) are used for attitude and coupled dynamic simulations. For a spin-stabilized sail, the SRPT should be zero to satisfy the torque balance, namely:

$$\boldsymbol{M}_s^b = 0. \tag{33}$$

The torque balance requires the cp and cm to accord with each other, which means that $\eta_i = 0$ $(i = 1, 2, 3)$.

5. Stability analysis

The stability of the coupled system is discussed for two cases: with and without cm/cp offset. For no cm/cp offset case, the attitude is independent of the orbit and the conclusion of Section 2 can be utilized to determine the stability of the coupled system. In this case, the orbit and attitude are analyzed separately. The orbit dynamics is discussed assuming that the attitude is in equilibrium and the attitude dynamics is discussed assuming that the orbit is evolving in the reference orbit. The coupled system is stable if both the orbit and attitude are stable. The coupled system is unstable if either the orbit or the attitude is unstable. For existing cm/cp offset case, no analytic conclusion can be utilized. Here, numerical simulations are used to illustrate the stability.

5.1. Stability of coupled system without cm/cp offset case

First, the orbit stability is analyzed. The reference orbit is the displaced orbit and it corresponds to an equilibrium point in the orbit frame. Once the orbit parameters are given, the corresponding required sail parameters and attitude parameters are determined. Eq. (13) is linearized around the reference orbit assuming that the attitude is in equilibrium. The solar radiation pressure acceleration is obtained by dividing the force in Eq. (22) by the mass. A position perturbation $(\,\delta\rho \quad \delta\vartheta \quad \delta z\,)$ is added to the displaced orbit. Then, the linear variational equations can be obtained as (McInnes, 1998):

$$\begin{cases} \delta\ddot{\rho} - \omega_0^2\delta\rho - 2\omega_0\rho_0\delta\dot{\vartheta} = \left[\tilde{\omega}^2(3\sin^2\gamma_0 - 1) + \frac{1}{m}\frac{\partial F_{sp}^o}{\partial\rho}\right]\delta\rho \\ \qquad\qquad + \left(3\tilde{\omega}^2\sin\gamma_0\cos\gamma_0 + \frac{1}{m}\frac{\partial F_{s\rho}^o}{\partial z}\right)\delta z, \\ \delta\ddot{\vartheta} + 2\frac{\omega_0}{\rho_0}\delta\dot{\rho} = 0, \\ \delta\ddot{z} = \left(3\tilde{\omega}^2\sin\gamma_0\cos\gamma_0 + \frac{1}{m}\frac{\partial F_{sz}^o}{\partial\rho}\right)\delta\rho \\ \qquad + \left[\tilde{\omega}^2(3\cos^2\gamma_0 - 1) + \frac{1}{m}\frac{\partial F_{sz}^o}{\partial z}\right]\delta z. \end{cases} \tag{34}$$

The derivatives of the SRPF with respect to orbit parameters are given by

$$\frac{1}{m}\frac{\partial F^o_{s\rho}}{\partial \rho} = -2\sin^2\gamma_0\left(\tilde{\omega}^2-\omega_0^2\right)+\frac{\cos\gamma_0}{mr_0^3}\frac{\partial Q_\rho}{\partial\gamma}, \tag{35}$$

$$\frac{1}{m}\frac{\partial F^o_{s\rho}}{\partial z} = -2\sin\gamma_0\cos_0\gamma\left(\tilde{\omega}^2-\omega_0^2\right)-\frac{\sin\gamma_0}{mr_0^3}\frac{\partial Q_\rho}{\partial\gamma}, \tag{36}$$

$$\frac{1}{m}\frac{\partial F^o_{sz}}{\partial \rho} = -2\sin\gamma_0\cos\gamma_0\tilde{\omega}^2+\frac{\cos\gamma_0}{mr_0^3}\frac{\partial Q_z}{\partial\gamma}, \tag{37}$$

$$\frac{1}{m}\frac{\partial F^o_{sz}}{\partial z} = -2\cos^2\gamma_0\tilde{\omega}^2-\frac{\sin\gamma_0}{mr_0^3}\frac{\partial Q_z}{\partial\gamma}, \tag{38}$$

$$\frac{\partial Q_\rho}{\partial\gamma} = \frac{P_0 l^2 AU^2}{2}\left(\frac{8}{3}\sin\gamma_0\cos\gamma_0\cos^3\varepsilon+\pi\cos^2\gamma_0\sin\varepsilon\cos^2\varepsilon -\pi\sin^2\gamma_0\sin\varepsilon\cos^2\varepsilon-4\sin\gamma_0\cos\gamma_0\sin^2\varepsilon\cos\varepsilon\right), \tag{39}$$

$$\frac{\partial Q_z}{\partial\gamma} = \frac{P_0 l^2 AU^2}{2}\left(\pi\sin\gamma_0\cos\gamma_0\sin\varepsilon\cos^2\varepsilon -2\pi\sin\gamma_0\cos\gamma_0\sin^3\varepsilon-4\sin^2\gamma_0\sin^2\varepsilon\cos\varepsilon +4\cos^2\gamma_0\sin^2\varepsilon\cos\varepsilon\right), \tag{40}$$

We may reduce this set of three coupled ordinary differential equations to two by integrating the second equation in Eq. (34) to obtain:

$$\delta\dot{\vartheta} = -2\frac{\omega_0}{\rho_0}(\delta\rho-\delta\rho_0). \tag{41}$$

Substitution of Eq. (41) into Eq. (34) adds a constant term, which does not influence the stability of the equilibrium point. Therefore, the initial derivation in radial direction is assumed to be zero, namely, $\delta\rho_0 = 0$. Then, the equation is written as:

$$\begin{cases}\delta\ddot{\rho} = K_{11}\delta\rho+K_{12}\delta z,\\ \delta\ddot{z} = K_{21}\delta\rho+K_{22}\delta z,\end{cases} \tag{42}$$

where the coefficients are given by

$$K_{11} = -\tilde{\omega}^2\left(3\sin^2\gamma_0-1\right)+\frac{1}{m}\frac{\partial F^o_{s\rho}}{\partial\rho}-3\omega_0^2, \tag{43}$$

$$K_{12} = 3\tilde{\omega}^2\sin\gamma_0\cos\gamma_0+\frac{1}{m}\frac{\partial F^o_{s\rho}}{\partial z}, \tag{44}$$

$$K_{21} = 3\tilde{\omega}^2\sin\gamma_0\cos\gamma_0+\frac{1}{m}\frac{\partial F^o_{sz}}{\partial\rho}, \tag{45}$$

$$K_{22} = \tilde{\omega}^2\left(3\cos^2\gamma_0-1\right)+\frac{1}{m}\frac{\partial F^o_{sz}}{\partial z}, \tag{46}$$

The stability characteristics of the system will be determined by the roots of the characteristic polynomial:

$$\lambda^4-(K_{11}+K_{22})\lambda^2+(K_{11}K_{22}-K_{12}K_{21}) = 0. \tag{47}$$

The characteristic polynomial has four complex roots, which represent four eigenvalues of the system. The coefficients of the polynomial are determined by two free parameters, $\omega_0/\tilde{\omega}$ and γ_0, where the ratio of ω_0 to $\tilde{\omega}$ determines the angular velocity of the displaced orbit and γ_0 describes the ratio of displaced height to orbit radius. The orbit size does not influence the stability. The stability characteristics of the families of displaced orbits may now be investigated by searching for regions with purely imaginary eigenvalues, $\lambda^2 < 0$ giving stable, bounded oscillations in the ρz plane. The stable regions are shown in Fig. 4. The stable region and unstable region are separated by two curves. The stable region expands as γ_0 increases. For a small γ_0, the orbit is only stable for a large orbit angular velocity.

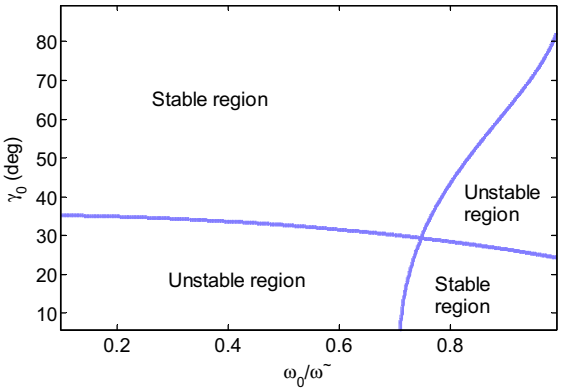

Fig. 4. Boundary between the stable and unstable regions.

The stable state of the attitude is that the sail spins along its symmetry axis, which can be described by the Euler angles and angular velocity. The reference spin angular velocity in the body-fixed frame is given by

$$\boldsymbol{\omega}^b = [\,0 \quad 0 \quad \omega_s\,]^T. \tag{48}$$

In this case, the SRPT is zero, namely, $\boldsymbol{M}_s^b = 0$. Eq. (32) can be simplified as:

$$\begin{cases}\dot{\omega}_x^b+\frac{(I_z-I_y)}{I_x}\omega_y^b\omega_z^b = 0,\\ \dot{\omega}_y^b-\frac{(I_z-I_x)}{I_y}\omega_x^b\omega_z^b = 0,\\ \dot{\omega}_z^b-\frac{(I_x-I_y)}{I_z}\omega_x^b\omega_y^b = 0.\end{cases} \tag{49}$$

The attitude dynamics is independent of the position and velocity of the sail. This is a classical spin-stabilized problem. If the sail is symmetric with respect to its spin axis, then, the inertia satisfies $I_x = I_y = I_t$. For spin-stabilized solar sail, the angular velocity satisfies $|\omega_x^b| \ll |\omega_z^b|, |\omega_y^b| \ll |\omega_z^b|$. Eq. (49) can be rewritten as:

$$\begin{cases}\ddot{\omega}_x^b+\frac{(I_z-I_t)^2}{I_t^2}\left(\omega_z^b\right)^2\omega_x^b = 0,\\ \ddot{\omega}_y^b+\frac{(I_z-I_t)^2}{I_t^2}\left(\omega_z^b\right)^2\omega_y^b = 0.\end{cases} \tag{50}$$

The solution is always stable since $(I_z - I_t)^2$ is positive. The stable solution is given by

$$\begin{cases}\omega_x^b = A_0\cos\left(\frac{I_z-I_t}{I_t}\omega_z^b t+\varphi_0\right),\\ \omega_y^b = A_0\sin\left(\frac{I_z-I_t}{I_t}\omega_z^b t+\varphi_0\right),\end{cases} \tag{51}$$

where

$$A_0 = \sqrt{\left[\omega_x^b(0)\right]^2+\left[\omega_y^b(0)\right]^2},$$

and $\tan\varphi_0 = \frac{\omega_y^b(0)}{\omega_x^b(0)}$ are determined by the initial values.

Eq. (51) shows that the sail attitude is always stable and the angular velocity perpendicular to the spin axis keeps small as long as it is small at initial time.

From above analysis we know that the orbit has stable regions and the attitude is always stable. From the conclusion in Section 2, the coupled system is stable if the orbit is chosen in the stable region. Therefore, the orbit in the unstable region can not be used without active control since it is unstable naturally. The active control of a spinning solar sail is more difficult than the control of a three-axis stabilization sail. With the consideration on the low sail film utilization efficiency, the active control of such a sail configuration is not a good option.

5.2. Stability of coupled system with cm/cp offset case

The center of mass and center of pressure can not be exactly the same because of all kinds of perturbations and fabrication errors. The difference between the cm/cp offset case and no cm/cp offset case is that the SRPT is zero or not. In the cm/cp offset case, the SRPT torque is not zero. Therefore, the attitude dynamics is different from no cm/cp case but the stability region for the orbit is not changed.

Assuming that Euler angles φ, θ are small, the SRPT generated by the cp/cm offset can be written as a polynomial of trigonometric functions:

$$\begin{cases} M_{sx}^b = g_x\left(\boldsymbol{r}_{pm}^b, \varepsilon, \gamma\right) \sin^{m_x}\psi \cos^{n_x}\psi, \\ M_{sy}^b = g_y\left(\boldsymbol{r}_{pm}^b, \varepsilon, \gamma\right) \sin^{m_y}\psi \cos^{n_y}\psi, \\ M_{sz}^b = g_z\left(\boldsymbol{r}_{pm}^b, \varepsilon, \gamma\right) \sin^{m_z}\psi \cos^{n_z}\psi, \end{cases} \tag{52}$$

where $g_{x,y,z}(\boldsymbol{r}_{pm}^b, \varepsilon, \gamma)$ is a constant function that depends on the cp/cm offset, half vertex angle, and sunlight angle of incidence. $m_{x,y,z}$ and $n_{x,y,z}$ are integers. The dynamic Eq. (32) can be rewritten as:

$$\begin{cases} \dot{\omega}_x^b + \frac{I_z - I_t}{I_t}\omega_s\omega_y^b = M_{sx}^b, \\ \dot{\omega}_y^b - \frac{I_z - I_t}{I_t}\omega_s\omega_x^b = M_{sy}^b, \\ \dot{\omega}_z^b = M_{sz}^b. \end{cases} \tag{53}$$

Since θ and φ are small, ω_x and ω_y are also small. The spin angular velocity is integrated assuming $\psi_0 = 0$ and $\psi = \omega_s t$. Substitution of $\psi = \omega_s t$ into Eq. (53) yields:

$$\dot{\omega}_z^b = g_z\left(\boldsymbol{r}_{pm}^b, \varepsilon, \gamma\right) \sin^{m_z}(\omega_s t)\cos^{n_z}(\omega_s t). \tag{54}$$

The equation is analytically integrable. The solution of angular velocity is bounded when $m_z + n_z$ is odd. And the angular velocity increases with time linearly if $m_z + n_z$ is even. Our case here belongs to the former case, $m_z + n_z$ is odd. Therefore, the angular velocity changes in the vicinity of its initial value. The maximum deviation from its initial value depends on the coefficient $g_z(\boldsymbol{r}_{pm}^b, \varepsilon, \gamma)$, which is very small here. It means that $\omega_z = \omega_s$ is a good approximation of the spin angular velocity. Substitution of it into the dynamics equation yields:

$$\begin{cases} \dot{\omega}_x^b + \frac{I_z - I_t}{I_t}\omega_s\omega_y^b = g_x\left(\boldsymbol{r}_{pm}^b, \varepsilon, \gamma\right) \sin^{m_x}(\omega_s t)\cos^{n_x}(\omega_s t), \\ \dot{\omega}_y^b - \frac{I_z - I_t}{I_t}\omega_s\omega_x^b = g_y\left(\boldsymbol{r}_{pm}^b, \varepsilon, \gamma\right) \sin^{m_y}(\omega_s t)\cos^{n_y}(\omega_s t), \end{cases} \tag{55}$$

Similarly, the solutions are periodic and bounded when $m_x + n_x$ and $m_y + n_y$ are odd. It is found that the indexes are also odd for SRPT in x^b and y^b direction. Therefore, the angular velocity is periodic and bounded. The magnitude of the variation depends on the initial value and coefficients g_x and g_y.

Above analysis shows that solar sail attitude is still stable for cm/cp case. However, there is no equilibrium point for the dynamic equations. The stability conclusions for a general solar sail in Section 2 is based on the Lyapunov stability theory. They can be used to determine the stability of equilibrium points. However, there is no equilibrium point for the coupled dynamical equations if a cm/cp offset exists for the solar sail. In this case, the conclusions in Section 2 can not be used to analyze the stability of the coupled system. Furthermore, it is difficult to determine the stability analytically since it related to the sail shape parameters and orbit parameters. Qualitative analysis shows that the SRPT generated by the cm/cp offset does change the attitude dynamic behavior much for this spin sail. The attitude behavior determines the orbit behavior. It is predicted that the coupled stability is not changed by the cm/cp offset. In

Table 2
simulation parameters for the orbit and attitude.

Case	Ix (kg m^2)	Iy (kg m^2)	Iz (kg m^2)	ε (rad)	γ_0 (rad)	r_0 (AU)	ω_0 (rad/s)	η_1 (m)	η_2 (m)	η_3 (m)	ω_s (rad/s)
A	1.3e4	1.3e4	4.3e4	0.3408	1.5658	0.98	ω_E	0	0	0	1e−2
B	1.3e4	1.3e4	4.3e4	0.3408	1.5658	0.98	ω_E	3	3	3	1e−2

Table 3
Initial attitude errors for the simulations.

Case	$\delta\varphi$ (rad)	$\delta\theta$ (rad)	$\delta\psi$ (rad)	$\delta\omega_x$ (rad/s)	$\delta\omega_y$ (rad/s)	$\delta\omega_z$ (rad/s)
A	1e−3	1e−3	1e−3	1e−4	1e−4	1e−4
B	1e−3	1e−3	1e−3	1e−4	1e−4	1e−4

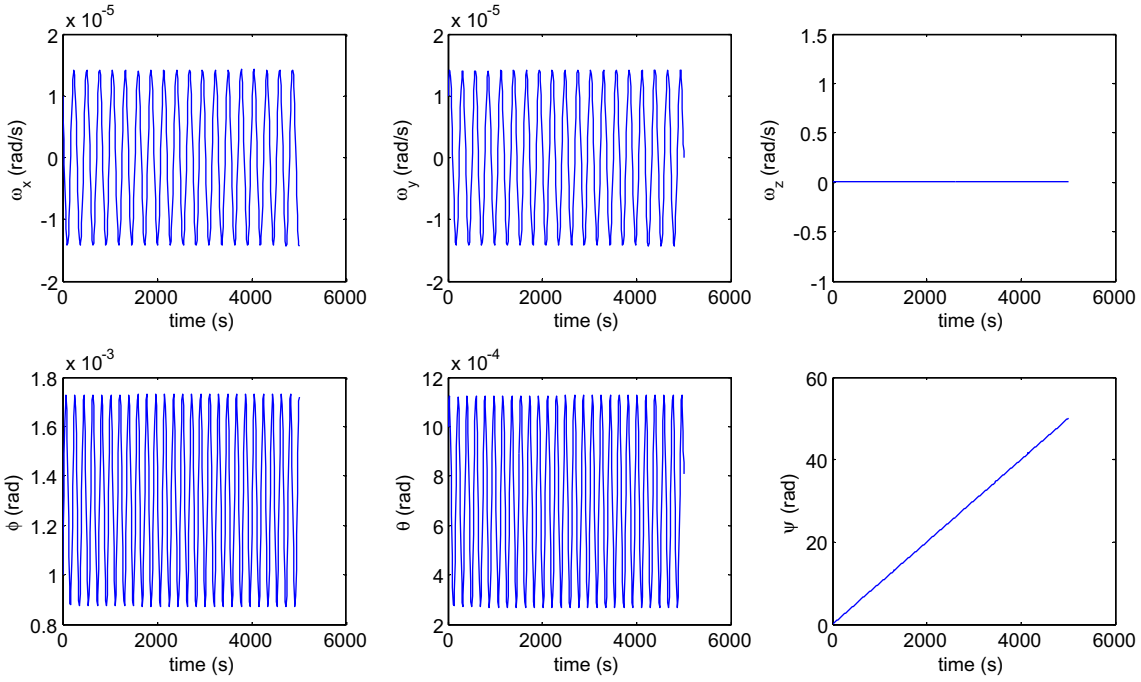

Fig. 5. Attitude responses of no cm/cp offset, case A.

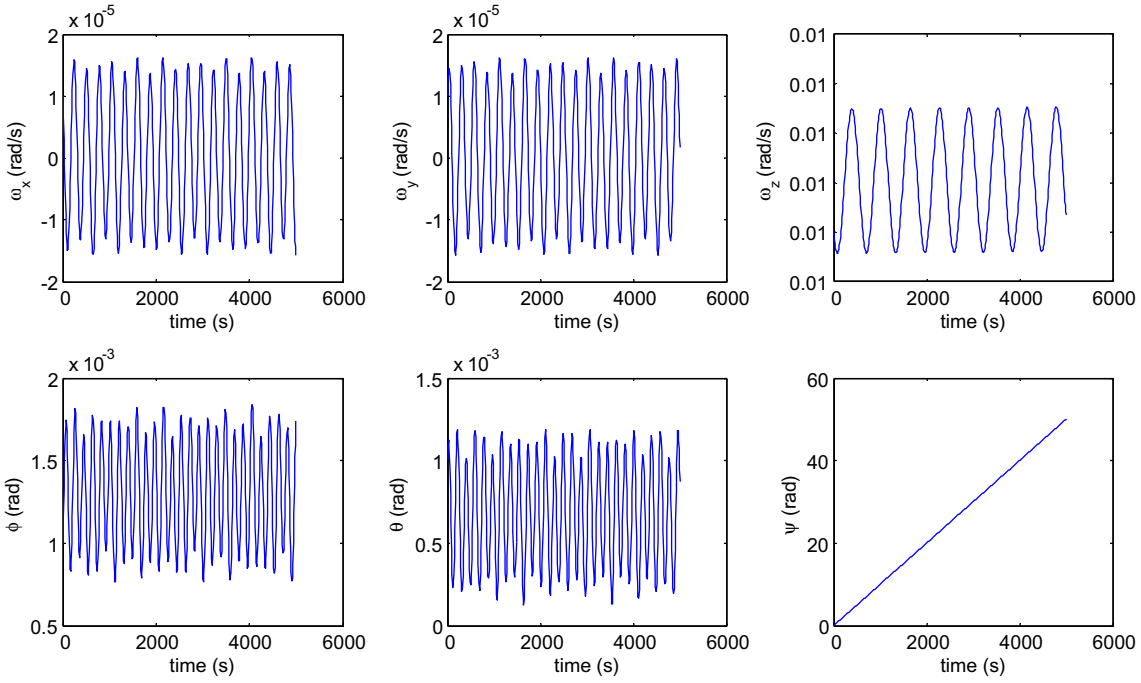

Fig. 6. Attitude responses of cm/cp offset, case B.

next section, numerical simulations are used to validate this prediction.

6. Simulations

The simulations are used to validate the analytical results and prediction above. The equations without any simplification are used for simulation. The simulation of the orbital dynamics is not given since the stability is analytically proved. The simulations of attitude dynamics for cm/cp case and no cm/cp case are given for comparison. Finally, a simulation of coupled dynamics is given to check the stability.

6.1. Attitude simulations

The attitude dynamics with and without cm/cp offset are investigated. The same spin angular velocity and initial

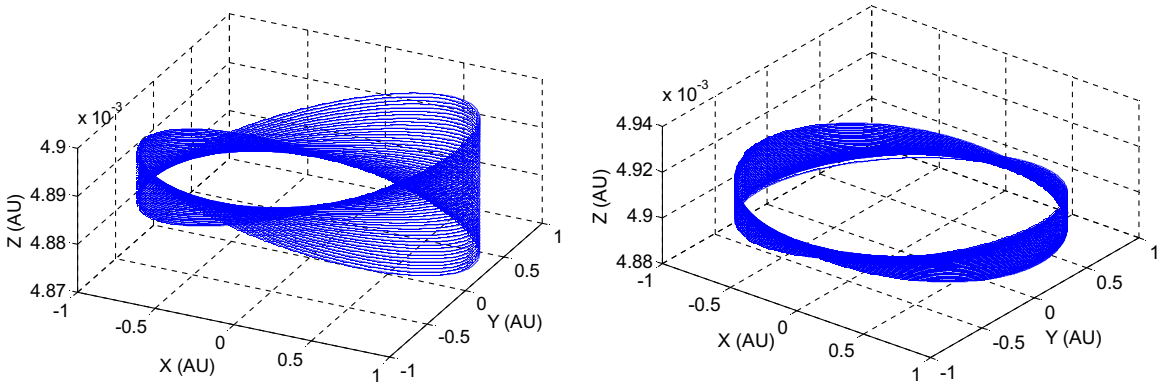

(a) Case A (b) Case B

Fig. 7. Orbit of the sail over 41 years.

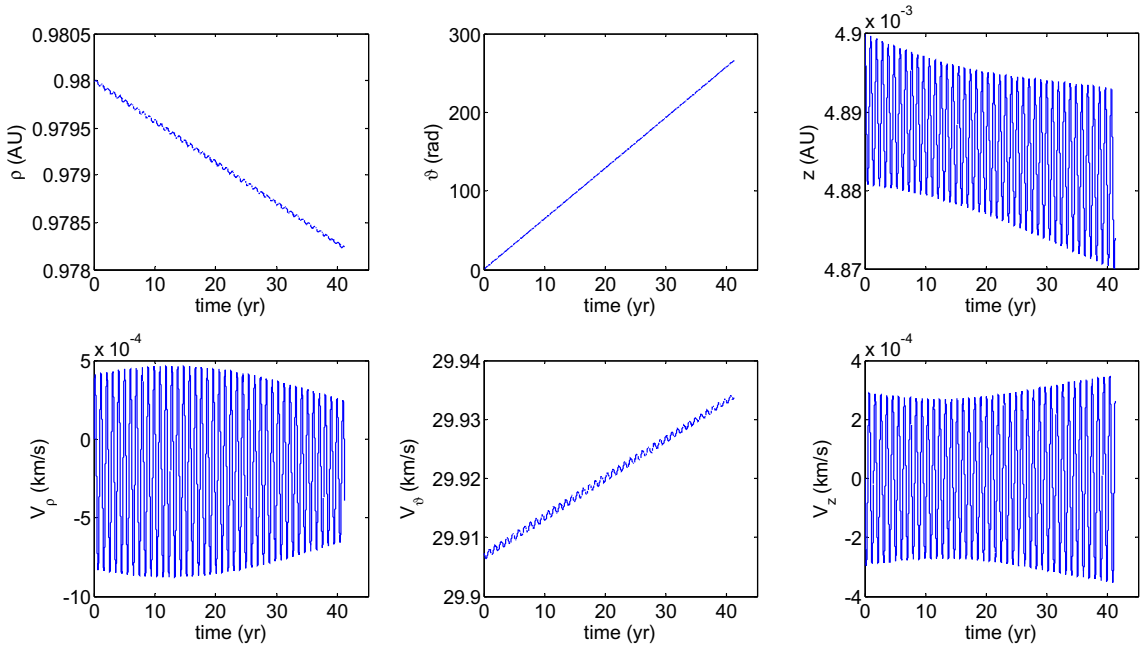

Fig. 8. Variations of orbit parameters of case A.

errors are used to check the stability of both cases. The attitude of no cm/cp offset case is always stable, the Euler angles and angular velocity vary in the vicinity of their reference values. The maximum derivation of the attitude from its reference value depends on the initial attitude error. For the case of existing cm/cp offset, the attitude is also stable when the initial attitude error is not very large (Euler angles less than 10°). For both cases, a precession of the sail with respect to the z axis will happen if initial attitude errors exist. The precession angle is determined by the initial attitude errors. Table 2 gives the parameters for simulations, where r_0 is the distance from the sail to the Sun and it is used to calculate the SRPT. Table 3 gives the initial attitude errors for the different simulation cases. The corresponding simulation results are shown in Figs. 5 and 6. As shown in Fig. 5 for no cm/cp case, the attitude motion is similar with a simple harmonic motion and the spin angular velocity keeps constant. As shown in Fig. 6, for cm/cp case, the SRPT will influence the frequency and amplitude of the attitude variation.

6.2. Coupled dynamics simulations

Similarly, the same parameters that appear in Tables 2 and 3 are used for coupled dynamics simulations. Here, the initial orbit errors are assumed several kilometers. Fig. 7 gives the sail orbit over about 41 years for cases A and B, respectively. The variations of the orbit radius and displaced height for both cases are shown in Figs. 8 and 9, respectively. For both cases, the displaced height vibrates in the vicinity of the reference height. The orbit radius decreases with time for no cm/cp offset case while

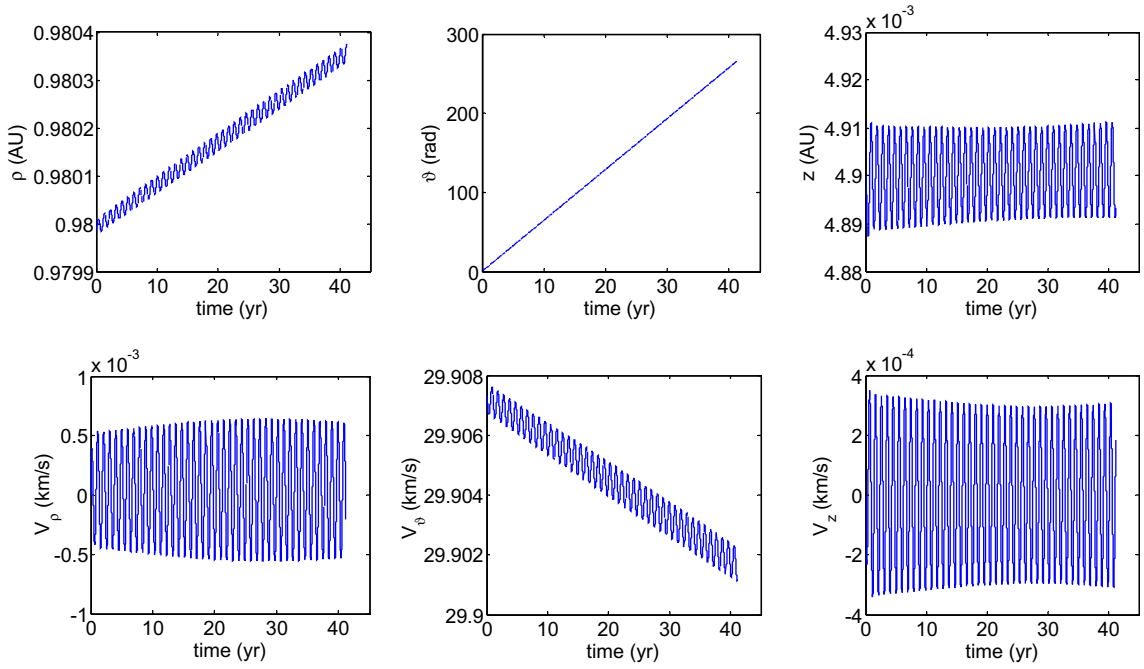

Fig. 9. Variations of orbit parameters of case B.

increases with time for cm/cp offset case. The rates of change for both cases are very small and the variation is less than 0.2% over 41 years. The orbit and attitude coupled system of no cm/cp offset case is stable since the orbit parameters lies in the stable region in Fig. 4. Therefore, the numerical simulation accords with the conclusion. The numerical results show that the orbit of cm/cp offset case is similar to the orbit of no cm/cp case. Therefore, the coupled system of this specific case is stable.

7. Conclusion

This paper gives the stability criterion for the attitude and orbit coupled system of a general solar sail. If the attitude of the sail is assumed to be independent of the orbit, the stability of the coupled system is determined by the stability of the attitude and orbit, respectively. Based on the stability criterion, a cone sail is proposed, which is spin-stabilized if the sail parameters are designed properly. The orbit dynamics of the sail in a heliocentric displaced solar orbit is discussed and the stable region is derived. The attitude dynamics and stability of the proposed cone sail are analyzed for the cases of existence of mass center and pressure center offset and non-existence of the offset. And the results show that the attitude is stable for both cases. For the case of no mass center and pressure center offset, it can be concluded that the coupled system is stable from the stability criterion. For the case of existence of the offset, analytical methods can not be employed to judge the stability of the coupled system. A numerical example is used to check the coupled dynamics. During the time of simulation, the orbit and attitude are stable for this case.

Acknowledgment

This work is supported by the National Natural Science Foundation of China (Grants Nos. 10902056 and 10832004) and Foundation from State Key Lab of Astronautical Dynamics (No. 2011ADL-DW0201).

References

Acord, J.D., Nicklas, J.C. Theoretical and practical aspects of solar pressure attitude control for interplanetary spacecraft, in: Progress in Astronautics and Aeronautics, Guidance and Control II. Academic Press, New York, 1964.

Benjamin, L.D. Attitude Control and Dynamics of Solar Sails. Thesis of M.S. Aeronautics and Astronautics Department, University of Washington, 2001.

Bong, W. Solar sail attitude control and dynamics, Part 1. Journal of Guidance, Control, and Dynamics 27, 526–535, 2004a.

Bong, W. Solar sail attitude control and dynamics, Part 2. Journal of Guidance, Control, and Dynamics 27, 536–544, 2004b.

Bong, W., David, M. Robust attitude control systems design for solar sail, part 1: proellantless primary ACS, in: AIAA Guidance, Navigation, and Control Conference and Exhibit, Providence, Rhode Island, 2004.

Forward, R.L. Light-levitated geostationary cylindrical orbits. Journal of the Astronautical Sciences 29, 73–80, 1981.

McInnes, R.C. The existence and stability of families of displaced two-body orbits. Celestial Mechanics and Dynamical Astronomy 67, 167–180, 1997.

McInnes, C.R. Passive control of displaced solar sail orbits. Journal of Guidance, Control, and Dynamics 21, 975–982, 1998.

McInnes, C.R. Solar sail mission applications for non-keplerian orbits. Acta Astronautica 45, 567–575, 1999.

McInnes, C.R. Non-keplerian orbits for mars solar reflectors. Journal of the British Interplanetary Society 55, 74–82, 2002.

McInnes, C.R., Macpherson, K.P. Solar sail halo trajectories: dynamics and applications, in: 42nd International Astronautical Congress, Montreal, IAF-91-334, 1991.

McInnes, C.R., Simmons, F.L. Solar sail halo orbits II: geocentric case. Journal of Spacecraft and Rockets 29, 462–479, 1992.

McInnes, C.R., Simmons, F.L. Solar sail halo orbits I: heliocentric case. Journal of Spacecraft and Rockets 29, 466–471, 1992.

Molostov, A.A., Shvartsburg, A.A. Heliocentric halos for a solar sail with absorption. Soviet Physics Dokladv 37, 149–152, 1992a.

Molostov, A.A., Shvartsburg, A.A. Heliocentric synchronous halos for a solar sail with absorption. Soviet Physics Doklady 37, 195–197, 1992b.

Prado, J.Y., Perret, A., Pignolet, G., Dandouras, I. Using a Solar Sail for a Plasma Storm Early Warning System. International Academy of Astronautics, Paper 96-IAA, 3.3.06, October 1996.

Sohn, R.L. Attitude stabilization by means of solar radiation pressure. Advances in Research Space 29, 371–373, 1959.

West, J.L. NOAA/DOD/NASA Geostorm Warning Mission. Jet Propulsion Lab, California Institute of Technology, Pasadena, CA, JPL D-13986, October 1996.